

Fuel Target Implosion

in Ion beam Inertial Confinement Fusion

Shigeo Kawata#

Graduate School of Engineering, Utsunomiya University
Utsunomiya 321-8585, Japan

The numerical results for the fuel target implosion are presented in order to clarify the target physics in ion beam inertial fusion. The numerical analyses are performed for a direct-driven ion beam target. In the paper the following issues are studied: the beam obliquely incidence on the target surface, the plasma effect on the beam-stopping power, the beam particle energy, the beam time duration, the target radius, the beam input energy and the non-uniformity effect on the fuel target performance. In this paper the beam ions are protons.

1. Introduction

In Ion Beam (IB) Inertial Confinement Fusion (ICF), the main research issues include 1) the IB production¹⁻³⁾ and the IB focusing, 2) the IB transportation⁴⁻⁹⁾ in an IB-ICF reactor and 3) the target physics, as well as 4) the reactor issues. The first and second points has been studied¹⁻⁹⁾. In this paper the third point of the fuel target physics is treated theoretically.

This paper presents the numerical analyses of the target implosion in IB ICF. In this paper IB means a proton beam. The numerical results are based on the one-dimensional (1-D)¹⁰⁾ computer code. In this paper the following important issues are focused and presented: 1) the IB oblique incidence to the target surface, 2) the plasma effect of the IB-stopping power, 3) the IB particle energy, 4) the IB time duration, 5) the target radius and 6) the IB input energy on the fuel target performance. The effects of the non-uniformity on the target implosion have been investigated already in another paper by 3-D numerical computations¹¹⁾. The results of the non-uniform implosion effect on the target performance are also briefly summarized at the end of this paper.

1. Fuel Target Implosion in IB ICF

The work was done in the author's Master (April, 1978 – March, 1980) and PhD (April, 1980 – October, 1981) courses at Tokyo Institute of Technology under the supervisor Prof. Keishiro Niu. The report was also included in the report on Heavy Ion Inertial Confinement Fusion Reactor System – HIBLIC (Nov., 1985), published by Nagoya University.

In this section, the characteristic phenomena of the IB target implosion are investigated mainly by the 1D fluid numerical analyses.

The target structure employed in the chapter is presented in Fig. 1. The ions deposit their energy in the tamper through the Coulomb-collisional-stopping power mainly. Therefore, the ion beams create the energy deposition Bragg peak in the Al layer in this specific target structure in Fig. 1. If the target has the structure shown in Fig. 1, the DT fuel is accelerated and compressed efficiently. The numerical computation code is described in the references 10-11).

At first, the typical numerical results are presented. The employed parameter values are listed in Table 1. Figures 2 show the stream lines and Fig. 3 show the space profiles of the ion temperature, the mass density and the pressure. Figure 4 shows the time sequences of the peak ion temperature of the DT fuel, the pellet gain Q (= the output fusion energy / the input IB energy E_b) and the density-radius product ρR . Figure 5 presents the implosion efficiencies. In Fig. 5 η_{imp} is defined by $(E_{\text{TDT}} + E_{\text{KDT}})/E_b$, η_{KDT} is defined by E_{KDT}/E_b and η_{Kin} is defined by $(E_{\text{KDT}} + E_{\text{KAlin}})/E_b$. Here E_{TDT} shows the thermal energy in the DT fuel, E_{KDT} the kinetic energy in the DT fuel and E_{KAlin} the kinetic energy, which is carried by the inward moving Al layer, that is a part of the payload. The implosion efficiency of η_{Kin} has a large value before the void closure time (τ_v). Before the void closure time, the DT fuel is compressed gradually. Then the void is closed and the fuel is compressed further more. These processes are presented in Figs. 2 and 6. In Fig. 6 the notation $\langle \alpha \rangle$ means the preheat ratio and is defined by (the spatially averaged ion temperature of the DT fuel at time (t) / the spatially averaged ion temperature estimated by the adiabatic relation from the initial ion pressure and the density at t).

2. IB Oblique Incidence on Target Surface

Usually the incident IB has the finite radius and the target is illuminated by the obliquely incident IB particles¹⁰. A part of the beam ions hits the target surface normally. But some of the beam ions hit the target surface obliquely. As the maximum incident angle θ_m increases, the Bragg peak becomes wide and the peak position moves outward in the target tamper as shown in Fig. 7. Therefore the material mass, which moves inward and is compressed with the DT fuel, becomes large as the increase in θ_m . This means that the implosion efficiency decreases with the increase in the incident angle. The relation between the implosion efficiency and θ_m is shown in Fig. 8. The numerical simulations are carried out in the case as shown in Table 2.

On the other hand, the ion energies of IB would be distributed in the range of Δe_b . It is clear that the broad energy deposition profile has the same effect as that of the IB incident angle (see Fig. 9).

In summary, M_{in} should be taken to be much less than M_{out} . Here M_{in} shows the total mass of the material, which moves inward including the DT fuel, and M_{out} the total mass of the

material which moves outward.

3. Plasma Effect on IB Stopping Power

During the IB illumination on the target, the target material is partially ionized. Therefore the free electrons, the bound ones and the ions contribute to the IB stopping power. Especially the plasma produced in the ion beam energy deposition layer behaves as not only the individual single particle gas but also the collective particle gas¹²⁾. The stopping power consists of the Coulomb collisional and the plasma wave one. Therefore the total stopping power increases and the stopping range decreases as the increase in the material temperature in the relatively low temperature range, for example, 0 to 300 eV for the typical case as shown in Fig. 10. From the considerations above and in this section 2, it seems to be apparent that the implosion efficiency becomes low, when the plasma effect on the stopping power is switched on.

In order to check the plasma effect on the target implosion, the numerical simulations are performed for two cases, which are the plasma effect-switched-on and -off ones, as shown in Table 3. As described above, the implosion efficiency η_{KDT} has a smaller value in the case in which the plasma effect is switched on, than that in the other case. However, it should be noted that η_{Kin} and η_{imp} have larger values in the former case than those in the latter. This fact can be explained by the following considerations: in the Al layer, the retained thermal energy, which can not contribute to the implosion until the void closure time, is presented by the notation of E_{TAl} in Table 3. The two values in the column of E_{TAl} are quite different with each other. In the case including the plasma effect, the IB input energy is used efficiently. This result can be explained as follows: when the shortening of the IB stopping range appears in the tamper or the energy deposition layer, the narrower region is heated and expands into the target radius size. Therefore, the thermal energy of the Al layer is converted efficiently to the kinetic energy. This fact leads to the higher implosion efficiency of η_{imp} in the case, in which the plasma effect is switched on.

In summary, the IB deposition region should be small in order to realize the efficient conversion from the thermal to the kinetic energy.

4. IB Particle Energy effect on target implosion

From the result in the above section 3, it is important that the IB energy should be deposited in the narrower region. In order to realize it, it seems to be better to take the lower particle energy e_b . Because the stopping range strongly depends on the IB particle energy.

In order to investigate the effect of the difference of the beam ion energy on the implosion, the computations of two cases in Table 4 are performed. As described above, E_{TAL} has the smaller value in the case of the lower e_b (=3MeV) than that in the other case e_b (=5MeV). This fact means that the IB input energy deposited in the Al layer is used more efficiently in the

case of $e_b=3\text{MeV}$. However, the implosion efficiency is small in the low e_b case, compared with that in the other case. This fact comes from the following two points: 1) the IB input energy into the Pb layer is larger in the low e_b case than the other, because in the low e_b case the deposition region is relatively narrow and the temperature increases rapidly in the deposition region. Therefore, the plasma effect affects strongly on the stopping range and the outer region is heated more. The total retained thermal energy E_T in the outer tamper region is large in the low e_b case, compared with the other. For the higher implosion efficiency it is important to convert the input energy E_b to the fuel kinetic energy efficiently. Therefore, E_T should be kept to be small. 2) Another important point is the preheat temperature T_{BT} of the DT fuel. The rapid increase of the pusher temperature leads to the appearance of the strong shock wave and the strong preheat. In the case of $e_b=3\text{MeV}$, T_{BT} has a larger value than that in the other. In order to realize the high density of the DT fuel the preheat temperature should be small.

In summary, it should be pointed out that the input energy should be deposited during a relatively long time interval for the high implosion efficiency and the high density.

5. IB Pulse Length

As shown in above section 4, it is important that the input energy is deposited during a relatively long time interval in the tamper. In Table 5, the comparison between two cases of $\tau_b=35.0\text{ nsec}$ and 55.0 nsec is presented. As is expected, the preheat temperature is low in the case of the long pulse duration, compared with that in the other case. But the implosion efficiency has a low value for the case of the short pulse duration. It is explained by the relation between the void closure time and the IB pulse length, as follows: For the longer IB pulse length, the input energy at the later stage of the IB time duration cannot be used effectively for the target implosion, because the only energy which is deposited far before the void closure time contributes to the implosion efficiently. While the input energy, which is deposited near or after the void closure time, cannot be converted to the fuel kinetic energy. In summary, it should be noted that the ion beam pulse duration must be much shorter than that of the void closure time.

6. Target Radius

The void closure time is strongly depends on the target radius, because the implosion velocity is nearly same in many usual cases and $\sim 3 \times 10^7\text{ cm/sec}$. Therefore, to realize the relation of $\tau_b < (\text{the void closure time } \tau_v)$, the large void or the large radius target should be chosen, except the considerations about the problems of the Rayleigh-Taylor (R-T) instability.

In Table 6, the numerical results are summarized for the comparison between the large and small void targets. As presented in Table 6, the implosion efficiencies and the other fusion parameters have the better values for the larger target. At the same time the non-uniformity

of the fuel implosion must be studied.

7. IB Input Energy

In Fig. 11, the target gain is plotted for the IB total input energy. In Fig. 11 only the DT total mass is optimized and the other parameters are shown in the figure. The gain curve is not flat and increases with the increase in the input energy. This fact comes from the following: the required minimum input energy is above ~several hundred kJ to 1 MJ for the fuel compression of the reactor size target. Therefore, it is pointed out that the larger input energy has an advantage to release the fusion energy in a fusion reactor system.

8. Discussions

In the above sections, the important issues are studied to obtain the sufficient target gain. In addition to above results, there are other points to be considered, for example, the total fuel mass and the R-T instability. If a target contains a too-much fuel for the fixed input energy, the fuel cannot be accelerated sufficiently, the implosion efficiency becomes lower and the ignition may not to be attained. Therefore, it is important to optimize the DT fuel mass for the high gain¹³⁾.

Another important issue is the uniform implosion. The R-T instability prevents the target uniform implosion and gives the upper limit for the target radius. The non-uniform beam illumination and the target non-uniformity itself also introduce the target non-uniform implosion. The numerical analyses for the effect of the non-uniform implosion on ρR have been done by the 3-D numerical computer code¹¹⁾. The previous results¹¹⁾ show that the restrictions for the non-uniformity of the implosion acceleration should be less than 2.7% for the volume compression ratio of 10000 or $\sim 3 - 6\%$ for 1000, as shown in Fig. 12.

Acknowledgements

The authors would like to present their appreciations to Prof. Keishiro Niu, who has passed away on April 17, 2012, for his strong encouragements for ion beam nuclear fusion. Prof. K. Niu has started the ion beam fusion since 1978 together with the authors in Tokyo Inst. of Tech., and has continued to encourage them to explore the ion beam inertial fusion.

References

- 1) K. Kasuya, K. Horioka, T. Takahashi, A. Urai and M. Hijikawa, Appl. Phys. Lett., 39 (1981)887.
- 2) S. Miyamoto, A. Yoshinouchi, et. al., Jpn. J. Appl. Phys. 22 (1983) L703.
- 3) P. A. Miller, et. al., Laser and Particle Beams, 2 (1984) 153.
- 4) S. Kawata, K. Niu and H. Murakami, Jpn. J. Appl. Phys., 22 (1983) 302.

- 5) J. R. Freeman, L. Baker and D. L. Cook, Nucl. Fusion, 22 (1982) 383.
- 6) H. Murakami, S. Kawata and K. Niu, Jpn. J. Appl. Phys., 22 (1983) 305.
- 7) D. G. Colombant, S. A. Goldstein and D. Mosher, Phys. Rev. Lett., 45 (1980) 1253.
- 8) S. Kawata and K. Niu, Laser and Particle Beams, 1 (1983) 121.
- 9) D. G. Colombant, S. A. Goldstein, NRL Memorandum Report 4640 (1981).
- 10) M. Tamba, N. Narata, S. Kawata and K. Niu, Laser and Particle Beams, 1 (1983) 121.
- 11) S. Kawata and K. Niu, J. Phys. Soc. Jpn., 53 (1984) 3416.
- 12) S. Ichimaru, *Basic Principles of Plasma Physics*, (W. A. Benjamin, 1973) P.64
- 13) S. Kawata and K. Niu, Res. Rep. in Inst. of Plasma Phy., Nagoya Univ., IPPJ-502 (1981).

Table 1 Parameter values employed in the numerical computations as the typical values. The notation C_{AL} shows the ratio of the deposited input energy in the Al layer to the total input energy E_b . The input beam power varies with $(time)^{2.5}$ from zero. The same time dependence of the IB input power is employed for the numerical computations through the paper.

INPUT BEAM ENERGY	E_b	5 MJ
BEAM-PROTON ENERGY	e_b	5 MeV
BEAM DURATION TIME	τ_b	35 nsec
MAXMAUM PROTON INCIDENT ANGLE	e_m	60 degrees
BEAM POWER		$t^{2.5}$
TARGET RADIUS	r_t	5 mm
	C_{AL}	0.8
TOTAL DT MASS	M_{DT}	1.0 mg

Table 2 Parameter values employed in the computations to check the effect of the IB oblique incidence to the target surface on the implosion performance.

INPUT BEAM ENERGY	E_b	7 MJ
BEAM-PARTICLE ENERGY	e_b	5 MeV
BEAM DURATION TIME	τ_b	35 nsec
BEAM POWER		$t^{2.5}$
TARGET RADIUS	r_t	5 mm
	C_{Al}	0.8
TOTAL DT MASS	M_{DT}	4.0 mg

Table 3 Numerical results. The parameter values employed are listed in the Table, and the others, which are not listed, are the same as those in Table 1.

PLASMA EFFECT ON BEAM STOPPING POWER

Target radius	r_t	=	5 mm
Particle energy	e_b	=	5 MeV
Beam energy	E_b	=	7 MJ
	C_{Al}	=	0.8
Beam duration time	τ_b	=	35 nsec

	θ_m	=	0.0	θ_m	=	60.0
	M_{DT}	=	4 mg	M_{DT}	=	2 mg
PLASMA EFFECT	ON		OFF	ON		OFF
η_{KDT} (%)	1.92		3.04	0.72		1.27
η_{Kin} (%)	10.6		7.0	10.9		9.07
η_{imp} (%)	7.4		4.62	4.33		4.17
M_{Alin} at τ_b (mg)	72.7		54.3	83.8		72.7
$M_{VAlin} + M_{VDT}$ at τ_v (g cm/s)	-7.93×10^5		-5.85×10^5	-7.16×10^5		-5.39×10^5
$\langle V_{DT} \rangle / 10^7$ (cm/s)	2.59		3.25	2.25		2.98
$\langle V_{in} \rangle / 10^7$ (cm/s)	1.03		1.02	0.834		0.722
τ_v (nsec)	46.6		37.0	51.1		43.4
$\langle T_{Al} \rangle$ at τ_v (eV)	205		364	155		259
E_{TAI} at τ_v (MJ)	2.41		4.30	1.82		3.06
Q	120		2.70×10^{-4}	77.3		68.5
ρR (g/cm ²)	13.8		7.16	22.0		13.7

Table 4. Numerical results. The computations are performed to check the effect of the difference of the particle energy e_b . E_{TAI} shows the retained thermal energy in the Al layer at the void closure time and E_{TPb} the thermal energy retained in the Pb Layer. $E_T = E_{TAI} + E_{TPb}$.

PARTICLE ENERGY (e_b) EFFECT

Target radius	r_t	=	5 mm
Beam input energy	E_b	=	5 MJ
Beam duration time	τ_b	=	35.0 nsec
Beam incident angle	θ_m	=	60.0
Total DT mass	M_{DT}	=	1 mg
	C_{Al}	=	0.8

Proton Particle energy e_b	5 MeV	3MeV
η_{KDT} (%)	0.44	0.794
η_{imp} (%)	4.92	3.23
η_{Kin} (%)	11.5	9.95
$\langle V_{DT} \rangle / 10^7$ (cm/s)	2.1	2.82
M_{Alin} (mg)	87.6	30.0
M_{Al} (mg)	110	47.5
M_{Pb} (mg)	106	50.8
$\frac{MPb + (MAL - MAlin) \times 100}{MPb + MAL + MDT} \%$	59.2	68.8
E_{TAI} at τ_v (MJ)	1.32	1.14
E_{TPb} at τ_v (MJ)	1.61	1.81
E_T at τ_v (MJ)	2.49	2.72
$\langle T_{DT} \rangle$ at τ_v (eV)	4.07	25.5
$\langle T_{Al} \rangle$ at τ_v (ev)	112	219
$\langle T_{Pb} \rangle$ at τ_v (ev)	174	342
τ_v (nsec)	55.5	46.6
Q	59	49
ρR (g/cm ²)	22.4	12.2

Table 5. Numerical results. The computations are carried out to investigate the effect of the difference of the LIB duration time on the implosion performance.

Beam DURATION (τ_b) EFFECT

Target radius	r_t	=	5 mm
	C_{Al}	=	0.8
Total DT mass	M_{DT}	=	1 mg
Beam input energy	E_b	=	5 MJ
Beam particle energy	e_b	=	5 MeV

Beam duration time τ_b (nsec)	35	55
η_{KDT} (%)	0.44	0.349
η_{imp} (%)	4.5	3.67
η_{Kin} (%)	11.4	7.85
$\langle T_{DT} \rangle$ at τ_v (ev)	4.07	2.86
$\langle V_{DT} \rangle / 10^7$ at τ_v (cm/s)	2.09	1.87
τ_v (nsec)	55.5	72.1
E_{TAL} at τ_v (MJ)	1.33	1.54
ρ_R (g/cm ²)	22.4	29.3
Q	59	59.5

Table 6. Numerical results. The computations are carried out to check the effect of the difference of the target radius on the implosion performance.

TARGET RADIUS (r_t) EFFECT

Total DT mass	M_{DT}	=	1 mg
	C_{Al}	=	0.8
Beam input enrgy	E_b	=	5 MJ
Beam particle enrgy	e_b	=	5 MeV
Beam duration time	τ_b	=	35 nsec
Beam incident angle	θ_m	=	60

Target radius r_t	(cm)	0.5	0.35
η_{KDT}	(%)	0.44	0.642
η_{imp}	(%)	4.5	4.34
η_{Kin}	(%)	11.4	6.8
$\langle V_{DT} \rangle 10^7$ at τ_v	(cm/s)	2.09	2.53
E_{TAI} at τ_v	(MJ)	1.33	1.42
τ_v	(nsec)	55.5	40.7
M_{Al}	(mg)	110	53
ρR	(g/cm ²)	22.4	15.1
Q		59	51.2

Target Structure for LIB Hollow Shell Target

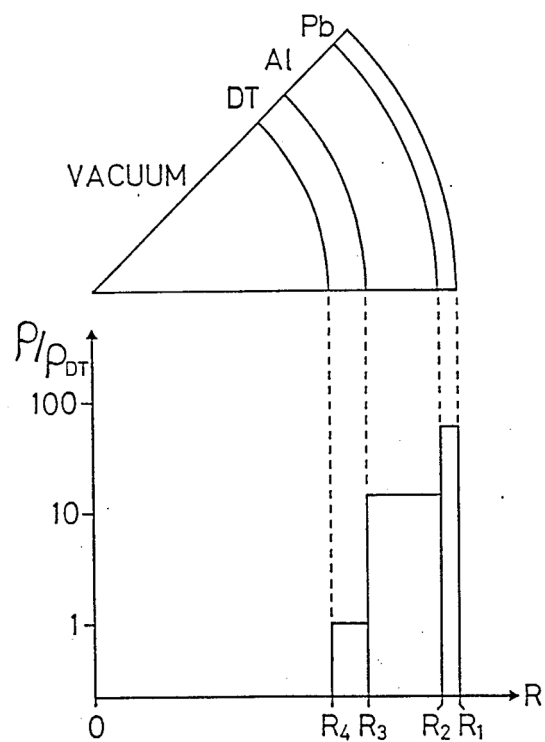


Fig. 1 The IB-target structure. The input IB deposits its energy mainly into the Al energy absorber layer.

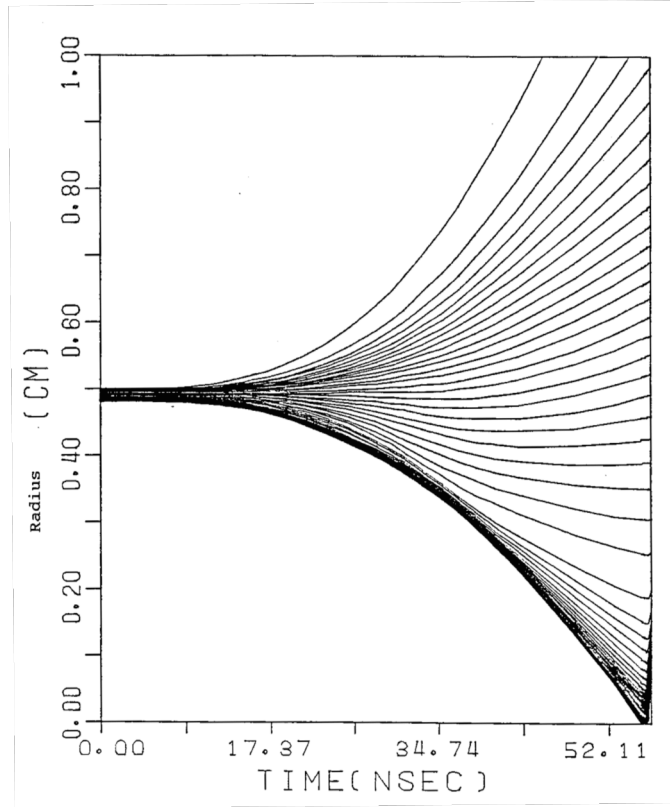


Fig. 2 The stream lines, obtained by the numerical computations in the case of the parameter values shown in Table 1. After the void closure time, the DT fuel is compressed further more by the A1 pusher.

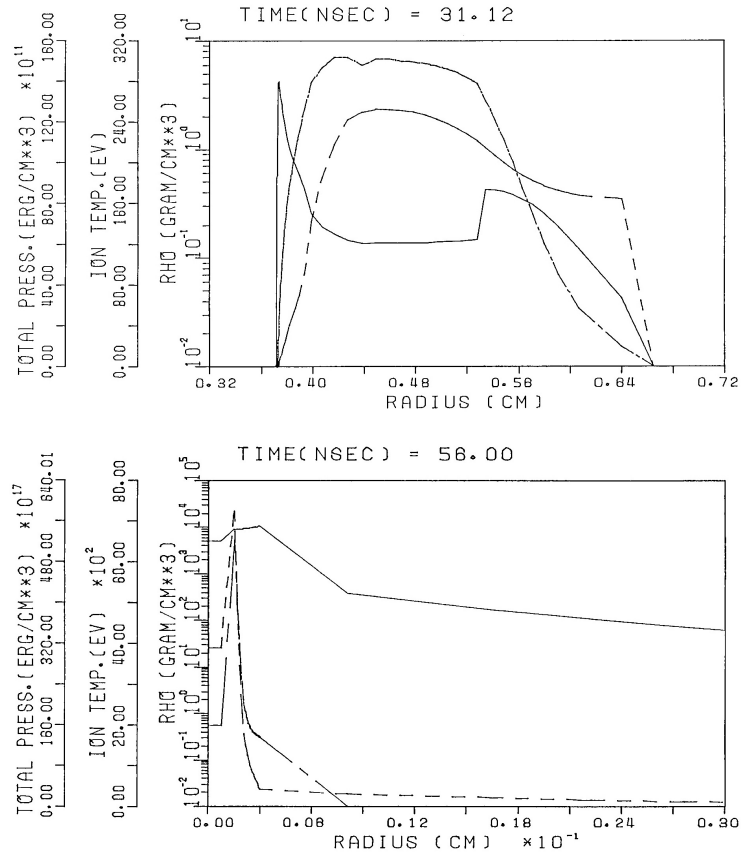


Fig. 3 The space profiles of the ion temperature T_i , the mass density ρ and the pressure P .

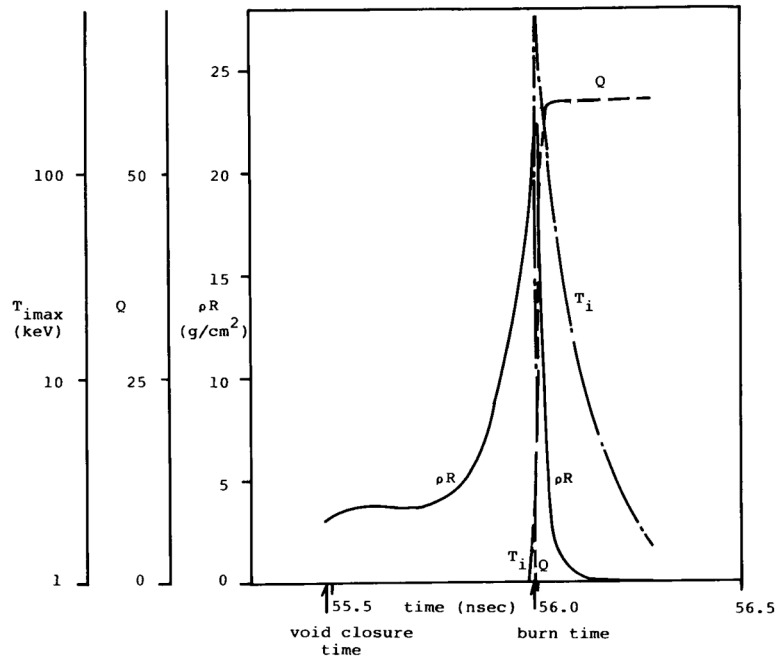


Fig. 4 The numerical results of the time sequences of the DT ion peak temperature, the pellet gain Q and the fuel density-radius product ρR .

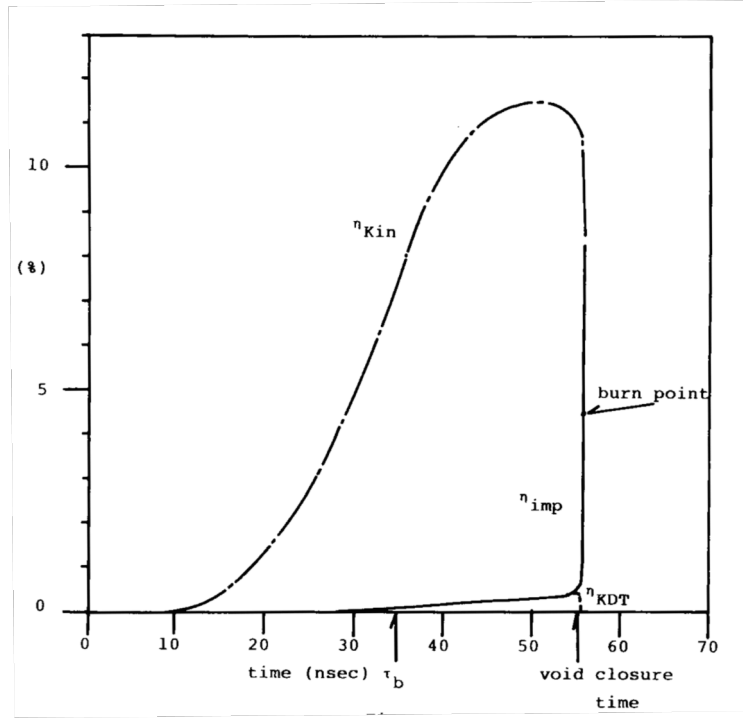


Fig. 5 Time histories of the implosion efficiency η_{imp} , the DT kinetic energy ratio η_{KDT} and ratio of the inward-moving kinetic energy η_{Kin} .

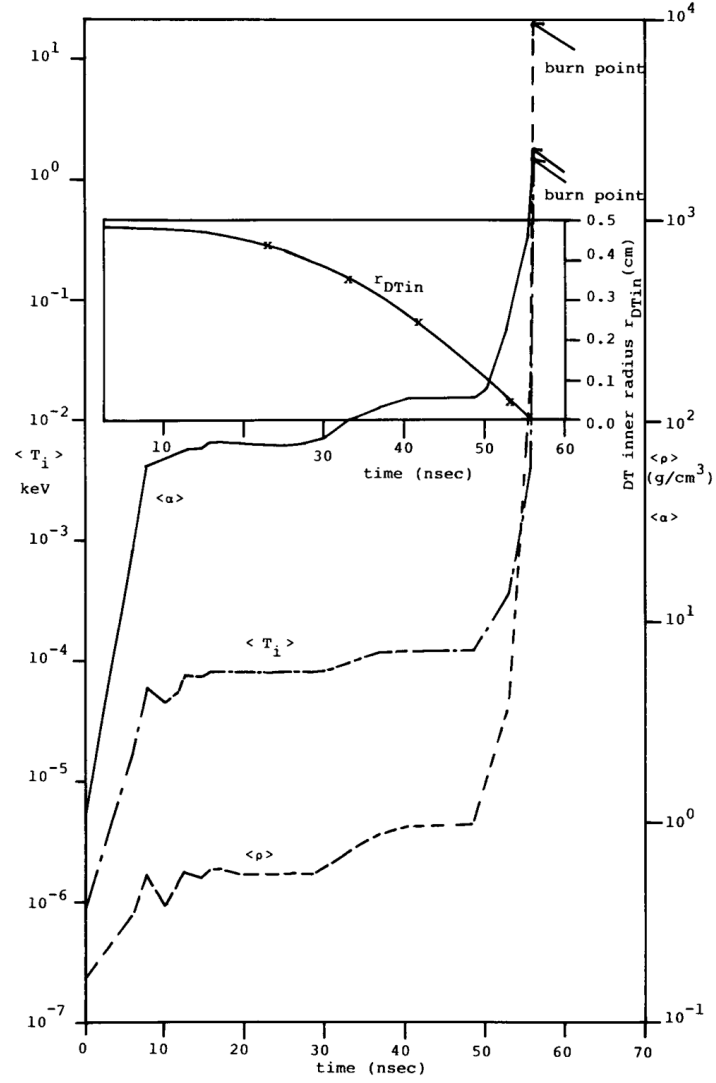


Fig. 6 DT fuel preheating feature. The notation $\langle \alpha \rangle$ is defined by (the spatially averaged ion temperature of DT fuel at time t) / (the spatially averaged ion temperature estimated by the adiabatic relation for the initial pressure and the density at t).

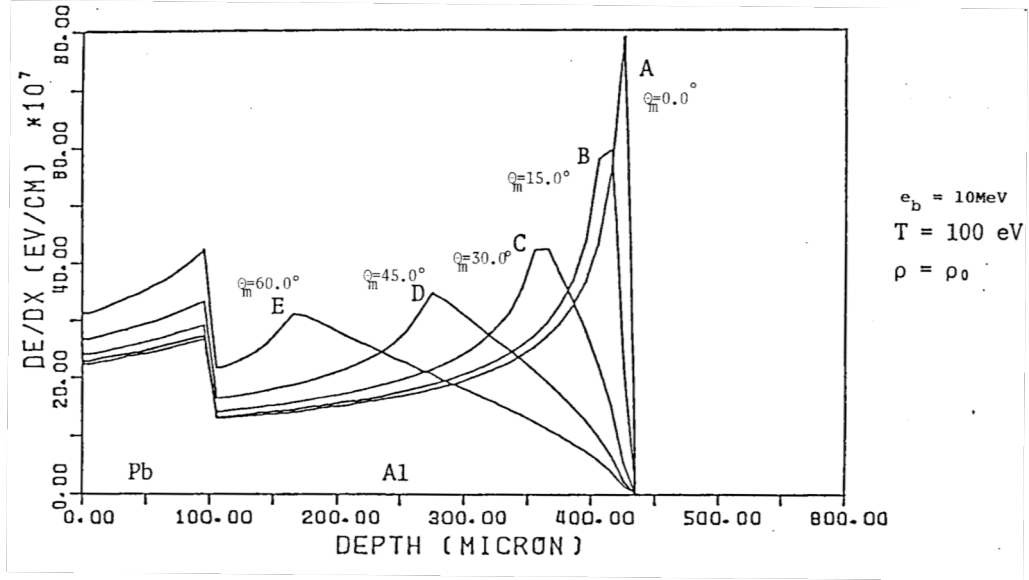


Fig. 7 The space profiles for the IB (ion beam) energy deposition. The profiles are computed by the following assumptions: the IB has the homogeneous distribution of the incident angle to the target surface normal in the azimuthal and polar directions, and the profiles are averaged in the both directions. In the figure, the target density is the solid one, the ion and electron temperatures 100eV and the input proton energy 10 MeV.

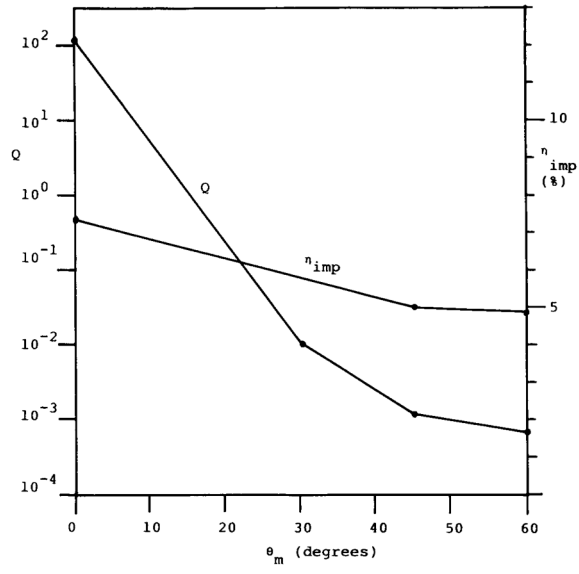


Fig. 8 The relation between the implosion efficiency η_{imp} and the incident angle θ_m . The pellet gain Q is also presented.

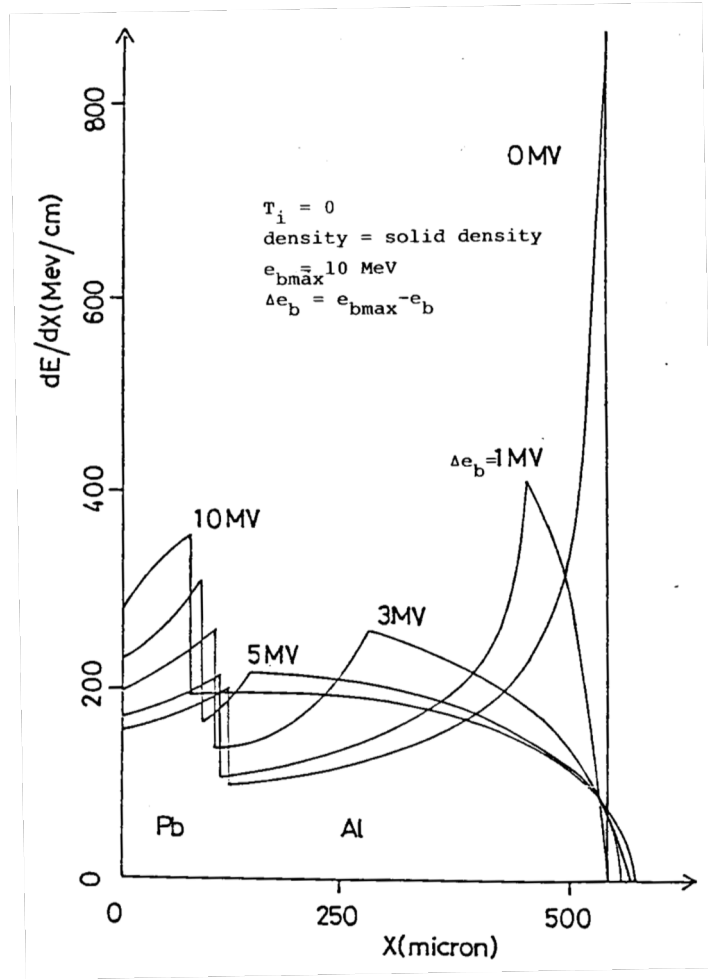


Fig. 9 The space profiles of the IB deposition energy. The input protons have the broad and homogeneous energy spectrum from e_b to $e_{bmax}(=10 \text{ MeV})$. The Δe_b is defined by $\Delta e_b = e_{bmax} - e_b$.

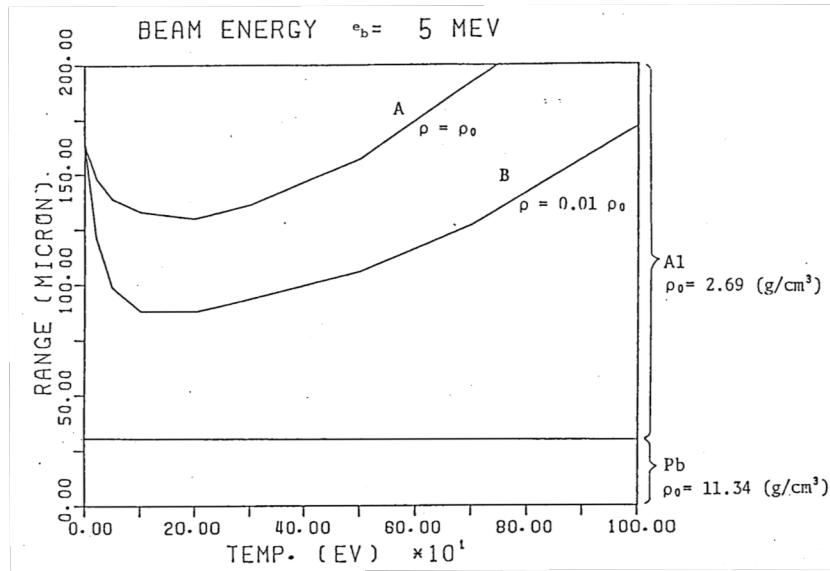


Fig. 10 The stopping range versus the target temperature. The stopping range shortening is clearly presented. The range shortening comes from the plasma effect of the stopping power.

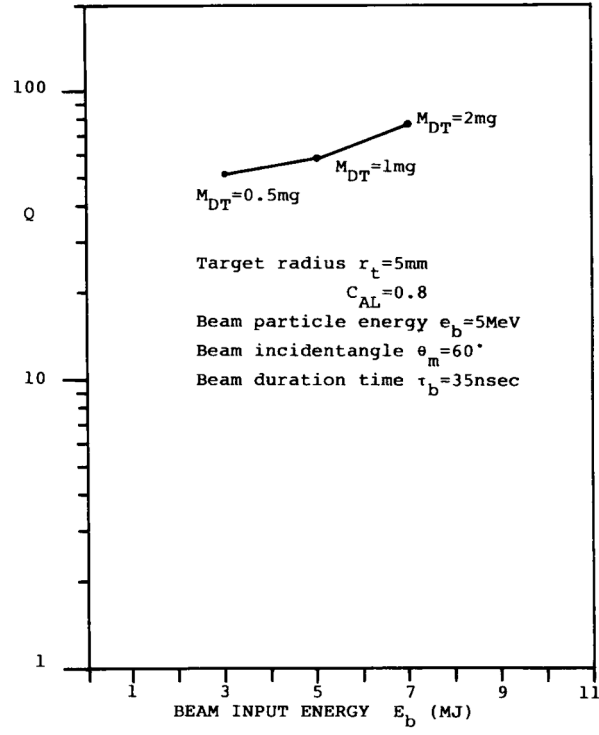


Fig. 11 The target gain Q versus the IB input energy E_b . In the figure the results are optimized only for the DT fuel total mass M_{DT} .

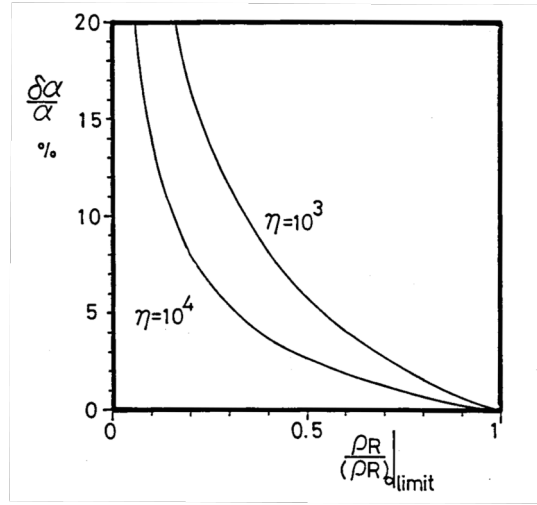


Fig. 12 The non-uniformity effect on the target implosion. The relation between the non-uniformity of the implosion acceleration $\delta\alpha$ and mass-density radius product ρR . In the figure η shows the volume compression ration (usually $\eta \sim 10^3 \sim 10^4$).